Acta Crystallographica Section D
Biological Crystallography
ISSN 0907-4449

Structure of the nucleotide-binding subunit B of the energy producer A_1A_0 ATP synthase in complex with adenosine diphosphate

Anil Kumar, Malathy Sony Subramanian Manimekalai and Gerhard Grüber*

Nanyang Technological University, School of Biological Sciences, 60 Nanyang Drive, Singapore 637551, Singapore

Correspondence e-mail: ggrueber@ntu.edu.sg

Received 17 July 2008
Accepted 1 September 2008

PDB Reference: A_1A_0 ATP synthase subunit B–ADP complex, 3dsr, r3dsrsf.

A_1A_0 ATP synthases are the major energy producers in archaea. Like the related prokaryotic and eukaryotic F_1F_0 ATP synthases, they are responsible for most of the synthesis of adenosine triphosphate. The catalytic events of A_1A_0 ATP synthases take place inside the A_3B_3 hexamer of the A_1 domain. Recently, the crystallographic structure of the nucleotide-free subunit B of *Methanosarcina mazei* Gö1 A_1A_0 ATP synthase has been determined at 1.5 Å resolution. To understand more about the nucleotide-binding mechanism, a protocol has been developed to crystallize the subunit B–ADP complex. The crystallographic structure of this complex has been solved at 2.7 Å resolution. The ADP occupies a position between the essential phosphate-binding loop and amino-acid residue Phe149, which are involved in the binding of the antibiotic efrapeptin in the related F_1F_0 ATP synthases. This trapped ADP location is about 13 Å distant from its final binding site and is therefore called the transition ADP-binding position. In the trapped ADP position the structure of subunit B adopts a different conformation, mainly in its C-terminal domain and also in the final nucleotide-binding site of the central $\alpha\beta$-domain. This atomic model provides insight into how the substrate enters into the nucleotide-binding protein and thereby into the catalytic A_3B_3 domain.

1. Introduction

Methanogens are able to grow by the conversion of a small number of compounds to methane. This rather simple pathway is not coupled to substrate-level phosphorylation but is instead coupled to the generation of ion gradients across the membrane. These ion gradients are used to drive the synthesis of adenosine triphosphate (ATP), which is catalyzed by the archaeal type A_1A_0 ATP synthases (A-ATP synthases; Schäfer *et al.*, 1999). The membrane-integrated enzyme is composed of subunits A–F, H, a and c with stoichiometry A_3:B_3:C:D:E:F:H_2:a:c_x (Coskun, Chaban *et al.*, 2004; Coskun, Radermacher *et al.*, 2004). Like the related bacterial F_1F_0 ATP synthases (F-ATP synthase; α_3:β_3:γ:δ:ε:a:b_2:c_x) and the eukaryotic V_1V_0 ATPases (V-ATPases; A_3:B_3:C:D:E_x:F:G_x:H:a:d:c_x:c'_x:c''_x), it possesses a water-soluble A_1 domain containing the catalytic sites and an integral membrane A_0 domain that is involved in ion translocation (Müller & Grüber, 2003). The primary structure of the archaeal ATP synthases is similar to that of the eukaryotic V-ATPases, but their function as an ATP synthase is more similar to that of the F-ATP synthases. ATP is synthesized or hydrolyzed on the A_1 headpiece, which consists of an A_3:B_3 domain, and the energy provided for or released during this process is transmitted to the membrane-bound A_0 domain. The energy coupling between the two active domains occurs *via* the so-called stalk sector (Müller & Grüber, 2003).

There are a total of six nucleotide-binding sites on A_1 and they are located in the A_3:B_3 sector (Schäfer *et al.*, 1999; Schäfer & Meyering-Vos, 1992). Of these, the three sites in subunit A have been described as having catalytic function (Schäfer *et al.*, 1999). Recently, the crystallographic structure of the nucleotide-free subunit A of *Pyrococcus horikoshii* A-ATP synthase has been solved at 2.55 Å resolution (Maegawa *et al.*, 2006). In contrast to subunit A, the nucleotide-binding subunit B does not contain the consensus sequences G*XX*G*X*GKTV, called the phosphate-binding loop (P-loop), and GER (Inatomi *et al.*, 1989), a phenomenon that they share with the eukaryotic V_1V_0 ATPases (Vasilyeva & Forgac, 1996). In comparison, these consensus sequences are conserved at the nucleotide-binding sites of the related α- and β-subunits of F-ATP synthases (Walker *et al.*, 1982; Saraste *et al.*, 1990). Based on the above facts, various suggestions have been made regarding the function and binding traits of subunit B in the A-ATP synthases (Schäfer & Meyering-Vos, 1992; Murata *et al.*, 2002; Schäfer, Bailer *et al.*, 2006) and V-ATPases (Vasilyeva & Forgac, 1996). Photoaffinity labelling (Schäfer, Rössle *et al.*, 2006; Schäfer & Meyering-Vos, 1992; Schäfer, Bailer *et al.*, 2006; Hosaka *et al.*, 2004) and fluorescence correlation spectroscopy experiments (Schäfer, Bailer *et al.*, 2006) have demonstrated that subunit B binds ATP analogues. Although it lacks the loop containing the G*XX*G*X*GKTV and GER sequences, the nucleotide-free atomic model of the A-ATP synthase subunit B showed that loops formed by the peptides $_{150}$SASGLPHN$_{157}$ and $_{184}$GIT$_{186}$ are present at corresponding positions in the structure of subunit B (Schäfer, Bailer *et al.*, 2006). The adenine-binding site in subunit B contains an aromatic Tyr338 and a basic Arg416 residue, which are predicted to undergo π–π stacking and cation–π interactions with the entering nucleotide, respectively.

Insight into the process of nucleotide entry requires diffraction-quality crystals of a nucleotide–protein complex. Here, we report the cocrystallization of ADP and subunit B of the A-ATP synthase from *Methanosarcina mazei* Gö1 and describe its structure at 2.7 Å resolution. For the first time, the nucleotide can be shown in a trapped transition ADP-binding position, which gives a clear picture about the path the nucleotide takes to enter the final substrate-binding site.

2. Experimental procedures

2.1. Crystallization of subunit B with ADP

Recombinant subunit B from *M. mazei* Gö1 was isolated according to Schäfer, Bailer *et al.* (2006). After purification, protein at a concentration of 3 mg ml^{-1} was incubated with 2 m*M* MgADP at 277 K for 30 min on a sample rotator and subsequently concentrated to 10 mg ml^{-1} using 30 kDa Centricon concentrators (Millipore). The protein–ligand complex was set up for crystallization in the final optimized condition [precipitant solution: 15%(*v*/*v*) glycerol, 20%(*v*/*v*) PEG 400, 0.1 *M* NaCl, 0.1 *M* sodium citrate pH 5.0 and 2 m*M* tris-(2-carboxyethyl) phosphine (TCEP)] in sitting-drop plates and incubated at 291 K.

2.2. Data collection and structure determination

A single crystal was harvested from the crystallization drop and was serially transferred using a nylon loop (Hampton Research) into cryoprotectant solutions comprising of 25%(*v*/*v*) glycerol, 20%(*v*/*v*) PEG 400, 0.1 *M* NaCl, 0.1 *M* sodium citrate pH 5.0 and 30%(*v*/*v*) glycerol, 20%(*v*/*v*) PEG 400, 0.1 *M* NaCl, 0.1 *M* sodium citrate pH 5.0. After soaking for 10 min in each cryoprotectant solution, the crystal was flash-frozen in liquid nitrogen at 100 K. A single-wavelength data set containing 90 images was collected by the oscillation method with a range of 1° per image using a wavelength of 1 Å with medium-energy radiation at 140 K on beamline 13B1 at the National Synchrotron Radiation Research Center (NSRRC; Hsinchu, Taiwan) using an ADSC Quantum 315 CCD area detector. The crystal diffracted to a maximum of 2.7 Å resolution and the data were indexed, integrated and scaled using the *HKL*-2000 suite of programs (Otwinowski & Minor, 1997).

Since the complex crystallized in the same space group and with similar unit-cell parameters as the nucleotide-free subunit B (Schäfer, Bailer *et al.*, 2006), this was used as a model for structure determination by the molecular-replacement method using the program *MOLREP* (Vagin & Teplyakov, 1997). The *R* factor for the best solution was 42.4%, with a correlation coefficient of 66.3%. After rigid-body refinement the initial *R* factor was 27.45%; at this stage, difference Fourier syntheses were calculated for the structure and the electron-density map clearly showed peaks corresponding to the bound ligand. To ascertain the presence of the bound ADP molecule in the complex, a series of simulated-annealing refinements were undertaken followed by OMIT-map calculations using the *CNS* program (Brünger *et al.*, 1998). Iterative cycles of model building and refinement were carried out using the programs *Coot* (Emsley & Cowtan, 2004), *CNS* and *REFMAC*5 (Murshudov *et al.*, 1997) from the *CCP*4 suite. NCS (noncrystallographic symmetry) and TLS (translation, liberation and screw) restrained refinements were used during structure refinement and the final model had an *R* factor of 19.8% and an $R_{\rm free}$ of 26.7%. The final electron-density map for the structure showed good density for most of the residues in both chains, with a few electron-density breaks. The geometry of the final model was checked using the program *PROCHECK* (Laskowski *et al.*, 1993), which gave good stereochemistry as can be noted from the Ramachandran plot, in which 99.2% of the main-chain torsion angles lie within the core region and the additionally allowed region. All the figures in the manuscript were drawn using the program *PyMOL* (DeLano, 2002).

2.3. Intrinsic fluorescence measurements of subunit B mutant F149W

To obtain a subunit B of the A_1A_0 ATP synthase from *M. mazei* Gö1 in which the occupancy of the transition ADP-binding position could be directly monitored, the subunit B mutant F149W, which has recently been generated (Kumar *et al.*, 2008), was used. A Varian Cary Eclipse spectrofluorometer

Table 1
Statistics of crystallographic data collection and refinement of ADP-bound subunit B.

Values in parentheses are for the last shell.

Wavelength (Å)	1.0
Space group	$P2_12_12_1$
Unit-cell parameters (Å)	a = 74.21, b = 95.94, c = 130.38
Resolution range (Å)	27.08–2.7
No. of unique reflections	23211
$I/\sigma(I)$	12.56 (2.7)
Completeness (%)	93.3 (78.5)
$R_{\rm merge}$† (%)	8.1 (45.8)
Multiplicity	3.7 (4.0)
Refinement statistics	
R factor‡ (%)	19.8
$R_{\rm free}$ (%)	26.7
Ramachandran statistics, residues in	
Most favoured region (%)	84.5
Additionally allowed region (%)	14.7
Generously allowed region (%)	0.8
Disallowed region (%)	0.0
R.m.s.d. from ideality	
Bond lengths (Å)	0.01
Bond angles (°)	1.44
B factor (Å^2)	
Mean overall	42.33
From Wilson plot	51.6

† $R_{\rm merge} = \sum_{hkl}\sum_i |I_i(hkl) - \langle I(hkl)\rangle| / \sum_{hkl}\sum_i I_i(hkl)$, where $\langle I(hkl)\rangle$ is the mean intensity for reflection hkl. ‡ R factor $= \sum ||F_{\rm o}| - |F_{\rm c}|| / \sum |F_{\rm o}|$, where $F_{\rm o}$ and $F_{\rm c}$ are measured and calculated structure factors, respectively.

was used and all experiments were carried out at 293 K. The samples were excited at 295 nm and the emission was recorded from 310 to 380 nm with excitation and emission band passes set to 5 nm.

3. Results and discussion

3.1. Structural features of subunit B in the presence of ADP

In order to understand the binding mode of the substrate ADP in the nucleotide-binding subunit B of the A-ATP synthase from *M. mazei* Gö1, we initiated a study of the three-dimensional structure of the protein–ligand complex. As detailed by Hassell *et al.* (2007), crystals of protein–ligand complexes can be obtained by (i) co-expression of the protein with the ligand, (ii) use of the ligand during protein purification, (iii) cocrystallization or (iv) soaking. Initially, soaking experiments were attempted with native crystals (Schäfer, Bailer *et al.*, 2006), varying the incubation time and the concentration of the ADP molecule, but these did not yield any successful results. Therefore, cocrystallization was initiated, wherein the ligand is added to the protein to form a complex that is subsequently used in crystallization trials. Various cocrystallization strategies such as incubating the ADP with the protein during protein purification were attempted. Many X-ray intensity data sets were collected to reasonable resolutions from crystals obtained under various conditions. However, in none of the data sets could positive electron density for the ADP molecule be observed at a reasonable σ cutoff. The third protocol, using the ligand before crystallization setups, was successful (see §2). Here, subunit B was incubated with ADP while it is in the dilute and monodisperse form before concentration to 10 mg ml^{-1}. The size of the crystals of the protein–ADP complex was improved by adjusting the glycerol concentration. Such crystals grew to dimensions of 0.07 × 0.04 × 0.03 mm over a period of three weeks and diffracted to 2.7 Å resolution. Like the nucleotide-free subunit B (PDB code 2c61; Schäfer, Bailer *et al.*, 2006), the ADP-bound form also crystallizes in the orthorhombic space group $P2_12_12_1$ with two molecules in the asymmetric unit, designated chain *A* and *B*, that are related by pseudo-twofold rotation (178.9°) in a head-to-tail orientation (Supplementary Figure S1[1]). The ADP molecule is bound between the two monomers, making maximum interaction with chain *A* rather than chain *B*. As in the structure of nucleotide-free subunit B (PDB code 2c61), the ADP-bound protein also consists of three domains: an N-terminal β-barrel (residues 13–76), an intermediate $\alpha\beta$-domain (residues 77–358) and a C-terminal α-helical bundle (residues 359–460) (Fig. 3*a*). The model of the ADP-bound subunit B comprises of 920 residues for both molecules in the asymmetric unit. No noticeable density was observed for residues 1–11, 60–69, 262–272, 307–312 and 458–460 in chain *A* and residues 1–10, 59–67, 263–268, 306–311 and 457–460 in chain *B*. About 402 water molecules could be identified in the nucleotide-bound structure. A detailed summary of the data-collection, phasing and structure-refinement statistics is given in Table 1.

The bound ADP molecule that lies near the P-loop region of the central $\alpha\beta$-domain has 50% occupancy, which was confirmed during the structure-refinement procedure. Multiple cycles of stimulated-annealing refinement with OMIT-map calculations were performed. The electron density of the ADP molecule could be identified at a 3σ cutoff in the ADP OMIT map (Fig. 1). The occupancy level of the bound ADP molecule was varied while checking its thermal parameters and the difference electron-density peaks during refinement and its final occupancy was estimated. The amino-acid residues that surround the ADP molecule within 5 Å are shown in Fig. 2. It could clearly be seen that the ADP molecule makes strong hydrogen-bonding interactions with the chain *A* residues, while the chain *B* residues play more of a supporting role by stabilizing the ADP molecule through weak van der Waals interactions. The phosphate groups of the ADP molecule are stabilized by hydrogen-bonding interactions with the main-chain atoms of the protein molecule. The O atoms of the β-phosphate of the ADP molecule form hydrogen-bonding interactions with the main-chain carbonyl O atoms of Ser304(*A*) and Pro315(*A*). The α-phosphate is stabilized by hydrogen-bonding interactions of its O atom with the main-chain amino N atom of Leu317(*A*) and the main-chain carbonyl O atom of Pro315(*A*). Thus, Pro315(*A*) makes a bifurcated hydrogen-bonding interaction with both phosphate groups of the ADP molecule. The ribose group of the ADP

[1] Supplementary material has been deposited in the IUCr electronic archive (Reference: MV5021). Services for accessing this material are described at the back of the journal.

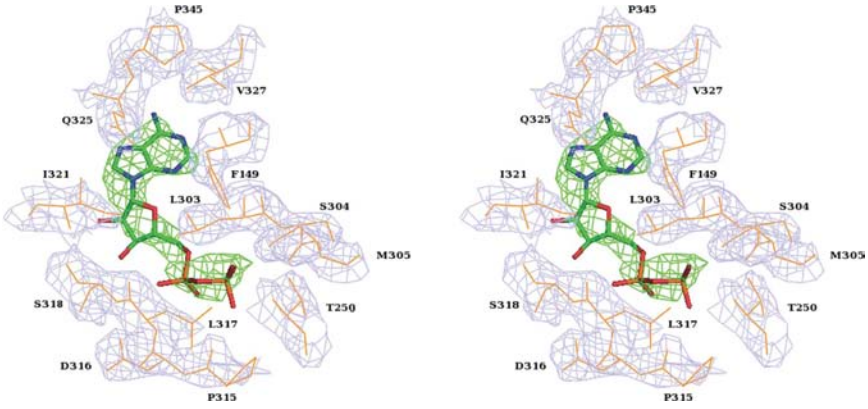

Figure 1
Stereoview of the ADP OMIT map. The difference $F_o - F_c$ electron-density map (green) for the ADP molecule is shown at the 3σ level. The $2F_o - F_c$ electron-density map (light blue) contoured at 1.5σ for some of the surrounding residues of subunit B is also shown.

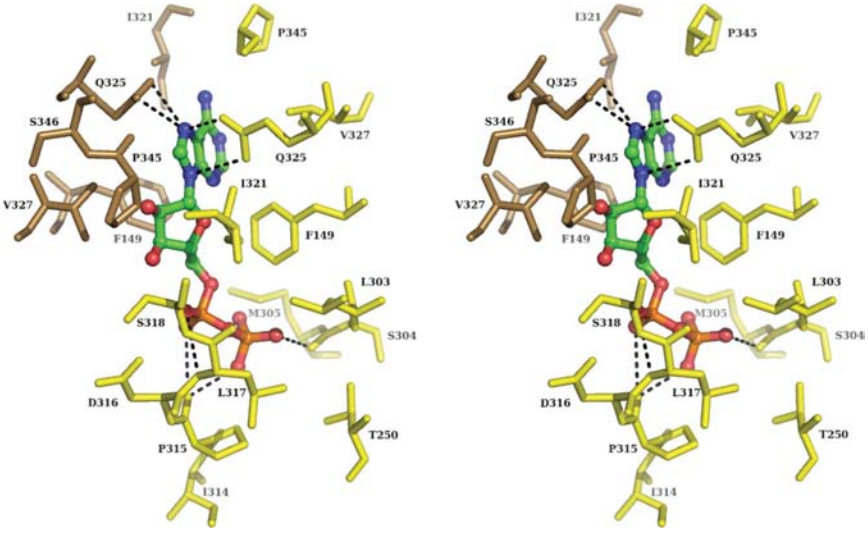

Figure 2
Stereoview of the amino-acid residues that surround the ADP molecule within a 5 Å radius. The ADP molecule is shown in ball-and-stick representation and the amino-acid residues are represented as sticks. Chain *A* residues are shown in yellow and chain *B* residues in brown. The hydrogen-bonding interactions between the ADP molecule and the amino-acid residues are shown as dotted lines.

molecule is mainly stabilized by hydrophobic interactions with the side-chain atoms of Ser318(*A*), Val327(*B*), Pro345(*B*) and Ile321(*A*). The adenine ring is stabilized by an offset $\pi\cdots\pi$ stacking interaction with Phe149(*B*) and an offset T-shaped $\pi\cdots\pi$ interaction with Phe149(*A*). In addition, the N atoms of the five-membered ring in the adenine group make a strong hydrogen-bonding interaction with the side-chain O and N atoms of Gln325(*A*) and Gln325(*B*), whereas one of the N atoms of the six-membered ring of the adenine group makes a hydrogen-bonding interaction with a water molecule. Furthermore, Val327(*A*), Pro345(*A*) and Ile321(*B*) make van der Waals interactions with the adenine group of the ADP molecule. All these interactions strongly hold the ADP molecule in its binding position, which is located about 13 Å apart from the final nucleotide-binding site and is made up by the phosphate-binding loop (P-loop) and the adenine-binding pocket (Schäfer, Bailer *et al.*, 2006; Fig. 3*a*).

3.2. Detection of ADP binding from the Trp fluorescence of subunit B mutant F149W

Recently, the Phe149 residue, which forms a $\pi\cdots\pi$ interaction with ADP (Fig. 3*a*), has been mutated to Trp (Kumar *et al.*, 2008). Here, we used this mutant to confirm that the trapped transition nucleotide-binding site is crucial for ADP binding. In this way, any nucleotide that interacts with this residue could be directly identified by its intrinsic fluorescence. As shown in Fig. 4, the absorbance spectrum of the F149W mutant protein shows a maximum at 336 nm. Addition of ADP lowered the fluorescence intensity by up to 18%. These data show that the trytophan fluorescence spectrum of mutant F149W is sensitive to ADP binding; therefore, the trapped nucleotide-binding position found in the present structure can be called an ADP transition binding state.

3.3. Structure comparison with nucleotide-free subunit B

The overall structure of the ADP-bound form is similar to that of nucleotide-free subunit B (PDB code 2c61), the r.m.s. deviation being 0.782 Å for the backbone C^{α} atoms. Notable deviations occur near the N-terminal region and in the loop regions Arg257–Tyr277 and Met305–Asp316. The maximum deviations are 5.5 Å for the Ala274 in the Arg257–Tyr277 region and 5.4 Å for Pro313 in the Met305–Asp316 region. These two regions are part of a loop region above the P-loop that would face the central stalk region in intact A_1A_0 ATP synthase. The latter region is also where the phosphate group of the ADP molecule binds and therefore this deviation could also be interpreted as being caused by ADP binding. The N-terminal β-barrel domain (13–76) of subunit B showed an r.m.s. deviation of 0.563 Å, whereas the central nucleotide-binding $\alpha\beta$-domain (77–358) showed a deviation of 0.888 Å and the C-terminal α-helical bundle domain (359–460) showed a deviation of 0.238 Å from the nucleotide-free structure. When the N-terminal domains of the two structures are superimposed [this domain was shown by Menz *et al.* (2001) to have the lowest mobility during nucleotide binding in the related F-ATP synthases] their C-terminal domains are related by a rotation of 3.5°. As can be seen in Fig. 3(*b*), the central $\alpha\beta$-domain show a slight deviation when compared with the

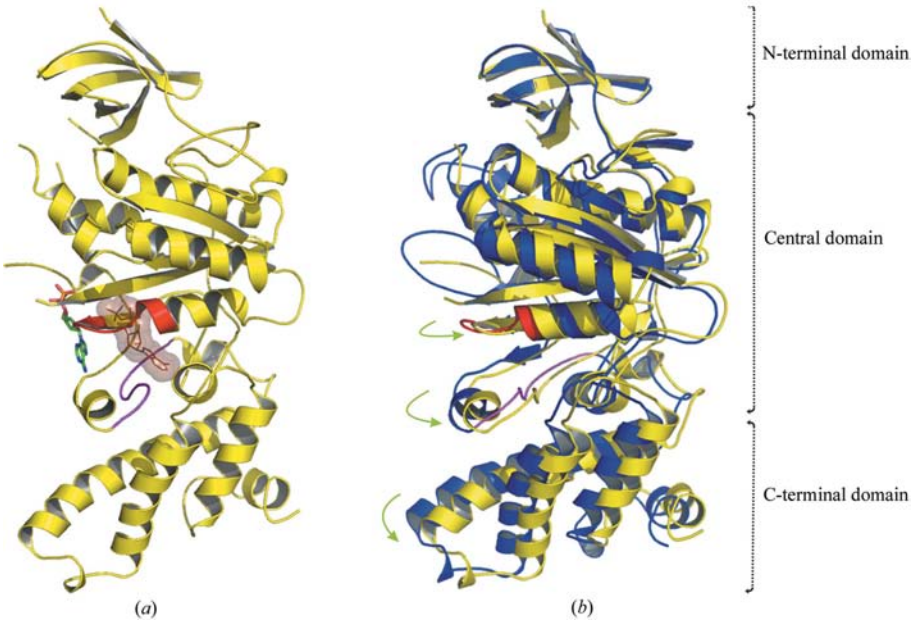

Figure 3
Structure of ADP-bound subunit B. (*a*) A cartoon representation of the structure of nucleotide-bound subunit B from *M. mazei* Gö1. The ADP molecule bound to the transition binding site is shown in green stick representation, while the actual site of ADP binding is shown by a brown surface with ADP docked inside. The P-loop region (Ser150–Glu158) is highlighted in red and the peptide Gly336–Arg349 that has been reported to covalently bind 8-N_3-3′-biotinyl-ATP (Schäfer, Bailer *et al.*, 2006) is shown in magenta. (*b*) Structure comparison of nucleotide-bound (yellow) and nucleotide-free (Schäfer, Bailer *et al.*, 2006; PDB code 2c61; blue) subunit B with respect to N-terminal domain superposition. The three domains of subunit B are marked. The green arrows represent the movement of the P-loop region, the peptide Gly336–Arg349 in the central $\alpha\beta$-domain and the C-terminal domain owing to the binding of the ADP molecule.

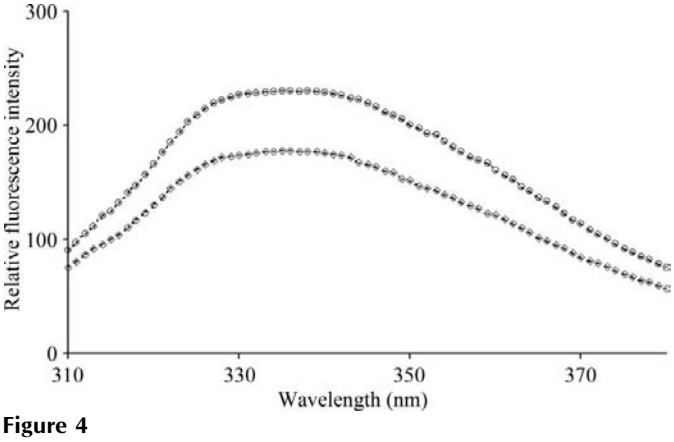

Figure 4
Fluorescence emission spectra of subunit B mutant F149W in the presence and absence of adenosine diphosphate. The fluorescence emission spectra (excitation wavelength of 295 nm with excitation and emission band passes of 5 nm) of mutant F149W were measured at 293 K. Fluorescence emission spectra of F149W mutant protein are shown in the absence (circles) and presence (diamonds) of 2 m*M* MgADP.

C-terminal domain, but significant movement is noted, especially in the lower part of the domain where the adenine-binding pocket is located. The region Glu323–Gly358 shows marked movement. Interestingly, this region includes the peptide Gly336–Arg349 that is reported to covalently bind 8-N_3-3′-biotinyl-ATP (Schäfer, Bailer *et al.*, 2006) and is the site of the adenine-binding pocket. The C-terminal α-helical domain deviates most and it moves as a rigid body. As has been demonstrated for the related F_1F_0 ATP synthases, the C-terminal domain of the β-subunit adopts different conformations depending upon whether or not a nucleotide is bound (Menz *et al.*, 2001). The nucleotide-free form (β_E) shows the highest mobility, which amounts to as much as a 33° rotation when compared with the nucleotide-bound form (β_{DP}). It has also been shown that the C-terminal domain moves slightly in the ADP-bound and phosphate-bound β_E structure, showing a 16° rotation owing to the binding of the nucleotide. In parallel with the above observation of movement of the C-terminal domain in the β-subunit of the F_1F_0 ATP synthases, we also observe rearrangements of the C-terminal domain in subunit B which might be caused by the binding of ADP. A structural alteration of the C-terminal domain of subunit B would be in accord with the rearrangements detected by cross-linking experiments of the entire methanogenic A_1A_0 ATP synthase, in which this C-terminal part moves relative to its neighbouring subunit F depending on whether ATP, ADP or ADP plus phosphate is bound to subunit B (Schäfer, Bailer *et al.*, 2006). Furthermore, a slight deviation in the P-loop region as well as a marked movement in the adenine-binding pocket is also noted, which might enable the ADP molecule to move from its transition position to the final adenine-binding site (Fig. 3*b*).

3.4. Biological relevance

The transition binding position of ADP in the present structure compares well with one of the inhibitory sites in the β-subunit of the F_1F_0 ATP synthase in which the antibiotic efrapeptin C, a potent inhibitor of ATP synthases in mitochondria and some bacterial species, binds (Supplementary Figure S2). Efrapeptin C is reported to interact with the adjacent α-subunit and the empty β-subunit, which might block the conversion of the β_E subunit from the open to the closed form and thereby inhibit enzyme activity (Abrahams *et al.*, 1996). The binding of efrapeptin takes place at helix G (residues 321–324) and strands 3 and 7 of the β-sheet (residues 151–155 and 302–309, respectively) in the central nucleotide-binding domain of β_E. When this domain is superimposed for the ADP-bound subunit B and β_E structures, the residues Phe149(*A*), Ser304(*A*), Met305(*A*), Ile321(*A*), Gln325(*A*), Val327(*A*) and Pro345(*A*), which are found to interact with

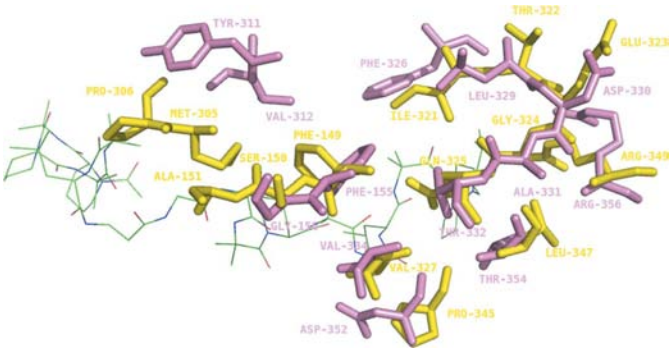

Figure 5
The efrapeptin-binding region of the β_E subunit of F-ATP synthase (pink; PDB code 1efr) overlapped with the nucleotide-bound subunit B (yellow) structure with respect to the central $\alpha\beta$-domain. The antibiotic efrapeptin (green) is shown as a line representation, while the amino-acid residues are shown in stick representation.

ADP in subunit B, also interact with efrapeptin. The side-chain orientations of three residues in the β_E subunit, Phe326, Asp352 and Arg356, are reported to affect efrapeptin binding and two of these residues have structural equivalents in the ADP-binding region of subunit B: Ile321(A) and Pro345(A) (Fig. 5). In the context of the data presented, we conclude that the mechanism of efrapeptin inhibition might be caused by its occupation of the transition binding position of ADP, hindering substrate entry into the regulatory/catalytic binding site.

In summary, the protocol developed for production of a subunit B–ADP complex enabled the solution of a high-resolution structure of the trapped transition ADP-binding position of subunit B. The structure adds to the understanding of how the substrate ADP enters into the nucleotide-binding subunit B of A-ATP synthase to reach its final binding site. This finding will also provide insight into the nucleotide-binding mode of the ADP/ATP-binding subunits of the related energy transducer V-ATPase and the prokaryotic and eukaryotic energy producer F-ATP synthase.

We thank the NSRRC (National Synchrotron Radiation Research Center) staff at beamline 13B1 for expert help with data collection. The NSRRC is a national user facility supported by the National Science Council of Taiwan. The Synchrotron Radiation Protein Crystallography Facility is supported by the National Research Program for Genomic Medicine. AK is grateful to the authority of Nanyang Technological University for the award of a research scholarship. This research was supported by A*STAR BMRC (06/1/22/19/467).

References

Abrahams, J. P., Buchanan, S. K., van Raau, M. J., Fearnley, I. M., Leslie, A. G. & Walker, J. E. (1996). *Proc. Natl Acad. Sci. USA*, **93**, 9420–9424.
Brünger, A. T., Adams, P. D., Clore, G. M., DeLano, W. L., Gros, P., Grosse-Kunstleve, R. W., Jiang, J.-S., Kuszewski, J., Nilges, M., Pannu, N. S., Read, R. J., Rice, L. M., Simonson, T. & Warren, G. L. (1998). *Acta Cryst.* D**54**, 905–921.
Coskun, Ü., Chaban, Y. L., Lingl, A., Müller, V., Keegstra, W., Boekema, E. J. & Grüber, G. (2004). *J. Biol. Chem.* **279**, 38644–38648.
Coskun, Ü., Radermacher, M., Müller, V., Ruiz, T. & Grüber, G. (2004). *J. Biol. Chem.* **279**, 22759–22764.
DeLano, W. L. (2002). *The PyMol Molecular Graphics System.* DeLano Scientific, Palo Alto, California, USA.
Emsley, P. & Cowtan, K. (2004). *Acta Cryst.* D**60**, 2126–2132.
Hassell, A. M. *et al.* (2007). *Acta Cryst.* D**63**, 72–79.
Hosaka, T., Murata, T., Kakinuma, Y. & Yamato, I. (2004). *Biosci. Biotechnol. Biochem.* **68**, 293–299.
Inatomi, K.-I., Eya, S., Maeda, M. & Futai, M. (1989). *J. Biol. Chem.* **264**, 10954–10959.
Kumar, A., Manimekalai, A. S. S., Balakrishna, A. M., Hunke, C., Weigelt, S., Sewald, N. & Grüber, G. (2008). In the press.
Laskowski, R. A., MacArthur, M. W., Moss, D. S. & Thornton, J. M. (1993). *J. Appl. Cryst.* **26**, 283–291.
Maegawa, Y., Morita, H., Iyaguchi, D., Yao, M., Watanabe, N. & Tanaka, I. (2006). *Acta Cryst.* D**62**, 483–488.
Menz, I. R., Walker, J. E. & Leslie, A. G. W. (2001). *Cell*, **106**, 331–341.
Müller, V. & Grüber, G. (2003). *Cell. Mol. Life Sci.* **60**, 474–494.
Murata, T., Yoshikawa, Y., Hosaka, T., Takase, K., Kakinuma, Y., Yamato, I. & Kikuchi, T. (2002). *J. Biochem.* **132**, 789–794.
Murshudov, G. N., Vagin, A. A. & Dodson, E. J. (1997). *Acta Cryst.* D**53**, 240–255.
Otwinowski, Z. & Minor, W. (1997). *Methods Enzymol.* **276**, 307–326.
Saraste, M., Sibbald, P. R. & Wittinghofer, A. (1990). *Trends Biol. Sci.* **15**, 430–434.
Schäfer, G., Engelhard, M. & Müller, V. (1999). *Mol. Biol. Rev.* **63**, 570–620.
Schäfer, G. & Meyering-Vos, M. (1992). *Biochim. Biophys. Acta*, **1101**, 232–235.
Schäfer, I., Bailer, S. M., Düser, M. G., Börsch, M., Ricardo, A. B., Stock, D. & Grüber, G. (2006). *J. Mol. Biol.* **358**, 725–740.
Schäfer, I., Rössle, M., Biuković, G., Müller, V. & Grüber, G. (2006). *J. Bioenerg. Biomembr.* **38**, 83–92.
Vagin, A. & Teplyakov, A. (1997). *J. Appl. Cryst.* **30**, 1022–1025.
Vasilyeva, E. & Forgac, M. (1996). *J. Biol. Chem.* **271**, 12775–12782.
Walker, J. E., Saraste, M., Runswick, M. J. & Gay, N. J. (1982). *EMBO J.* **1**, 945–951.